# A Miniaturized Transcutaneous Carbon Dioxide Monitor Based on Dual Lifetime Referencing

Tuna B. Tufan

Electrical and Computer Engineering Worcester Polytechnic Institute, Worcester, MA 01609 Email: ttufan@wpi.edu Ulkuhan Guler

Electrical and Computer Engineering Worcester Polytechnic Institute, Worcester, MA 01609 Email: uguler@wpi.edu

Abstract—The ability to monitor blood gases, namely oxygen and carbon dioxide, in real-time is of critical importance to clinicians in diagnosing and treating respiratory disorders. Transcutaneous monitors measure the partial pressure of carbon dioxide diffused from the skin. These monitors are noninvasive and capable of continuously monitoring carbon dioxide. Conventional transcutaneous carbon dioxide monitors require a heating element and large calibration equipment for reliable measurements. We propose a miniaturized transcutaneous carbon dioxide monitor based on a luminescence sensing film and dual lifetime referencing technique to assess the partial pressure of carbon dioxide within the 0-75 mmHg range, covering the clinically relevant range for healthy humans, 35-45 mmHg. We measured the partial pressure of carbon dioxide with less than  $\sim 1.6\,\%$  error in the given range without any post-processing and heating.

#### I. INTRODUCTION

Along with oxygen  $(O_2)$ , carbon dioxide  $(CO_2)$  is a key substance found in human vessels, often called blood gases, that reflects the status of respiratory functions [1], [2]. Abnormal respiratory conditions causing significant variations in the partial pressure of carbon dioxide in arteries  $(PaCO_2)$  lead to severe respiratory and neurological complications such as blackout, seizures, and brain injury, especially in preterm neonates [3], [4]. Noninvasive monitoring of  $CO_2$  enables clinicians to observe the trends and respond to fluctuations promptly, unlike the gold standard arterial blood gas analysis (ABG), which is inconvenient for frequent sampling of  $PaCO_2$  [5], [6]. Transcutaneous monitoring is a noninvasive technique to measure  $CO_2$  that diffuses from the skin, namely partial pressure of transcutaneous carbon dioxide  $(PtcCO_2)$ .  $PaCO_2$  can be derived from  $PtcCO_2$  with a linear relation [7], [8].

Traditional transcutaneous sensors, based on electrochemical electrodes [9], rely on a heating element and a bulky gas bottle for accurate measurements and calibration. The concerns about traditional sensors' size, heating, and power consumption make them unsuitable for long-term, continuous monitoring. Multiple studies have investigated alternative sensing methods for wearable applications, such as the infrared (IR) absorption principle of CO<sub>2</sub> [10]–[12] or CO<sub>2</sub>-sensitive luminescent sensors [13], [14]. For the IR-based solutions, the sensing range depends on the optical path. Therefore,

This material is based upon work supported in part by the National Science Foundation (NSF) under Grant EECS-2143898. Corresponding author: Ulkuhan Guler: uguler@wpi.edu.

optimizing the sensing range often leads to bulky or complex gas chamber designs [15], [16], hard to implement as wearable.

We present a luminescent film based PtcCO<sub>2</sub> monitor which utilizes dual lifetime referencing (DLR) technique to sense CO<sub>2</sub>. This paper demonstrates the feasibility of a miniaturized wearable, implementing the DLR technique. The rest of the paper is organized as follows. Section II gives the background on DLR and the motivation behind choosing this method. Section III explains the system architecture and how different DLR schemes are implemented in detail. Section IV discusses the measurement results, and Section V concludes this paper.

### II. DUAL LIFETIME REFERENCING

Luminescent materials emit light from electronically excited states; a phenomenon called luminescence. The excitation occurs when the material is exposed to photons of a specific wavelength. Absorption of these photons leads to luminophores in the luminescent material being excited to a higher energy state from the ground state. Based on the type of the excited state, the luminescence is categorized as fluorescence or phosphorescence. In fluorescence, a fluorophore transits back to the ground state within nanoseconds and emits a photon. Emitted photons have less energy than the photons of excitation; therefore, they are longer in wavelength. Luminescent materials are often sensitive to analytes, decreasing the emission intensity; this process is called quenching [17]. In the case of proposed application, the analyte is CO<sub>2</sub>.

The emission intensity is proportional to CO<sub>2</sub> partial pressure (PCO<sub>2</sub>) in the environment and can be used to monitor variations in PCO<sub>2</sub>. However, the emission intensity can be altered by confounding factors such as the excitation intensity, detector's photo-sensitivity, or the luminescent material's photo-bleaching. The lifetime of the emitted photons is another parameter that relates to PCO<sub>2</sub>. Lifetime measurement yields more accurate results as it is insensitive to such confounding factors. However, CO<sub>2</sub> sensors are fluorescent; hence the lifetime of the fluorophores is in the nanosecond regime [18], which complicates the design of the readout electronics.

Alternatively, the DLR technique incorporates a secondary luminophore, insensitive to the analyte, that has a significantly longer lifetime (typically in  $\mu$ s regime) than that of an analytesensitive fluorophore with a short lifetime [19]. The idea behind DLR is to use a secondary luminophore as a reference,

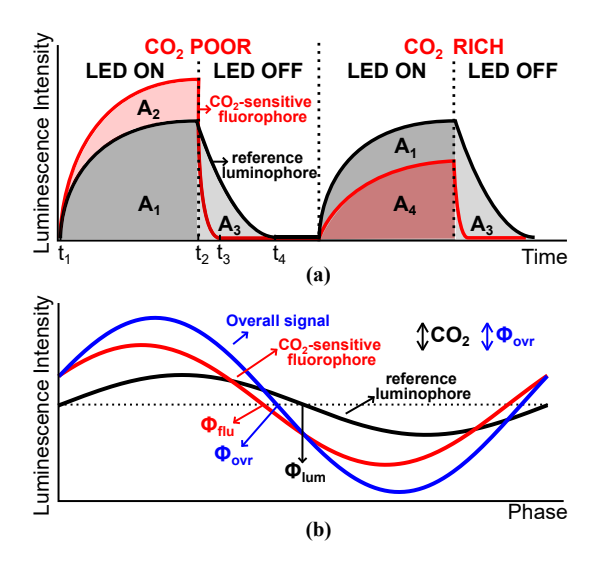


Fig. 1. (a) Time-domain and (b) frequency-domain dual lifetime referencing.

equally affected by the confounding factors, and cancel out these factors by taking the ratio of the luminescence of both the  $CO_2$ -sensitive fluorophore and the reference luminophore. There are two approaches: the time-domain DLR (t-DLR) and frequency-domain DLR (f-DLR).

In t-DLR, the luminescence is captured during the LED is ON and after it is turned OFF. The components of the luminescence are analyzed separately in Fig.1.a. When the LED is ON, the luminescence is the combination of emission of both CO<sub>2</sub>sensitive fluorophores and reference luminophores. The total luminescence,  $A_{on}$ , is equal to the sum of the areas under the fluorophore  $(A_2)$  and luminophore curves  $(A_1)$  from time  $t_1$  to  $t_2$ ,  $(A_{on}=A_1 + A_2)$ . However, when the LED is turned OFF, the reference luminophores dominate as the CO<sub>2</sub>-sensitive fluorophores decay rapidly and have a significantly shorter lifetime  $(t_4-t_2\gg t_3-t_2)$ . Therefore, the total luminescence during this period,  $A_{off}$  is the area under the luminophore curve  $(A_3)$ from  $t_2$  to  $t_4$ ,  $(A_{off}=A_3)$ . Furthermore, exposing the sensor to more CO<sub>2</sub> decreases the luminescence of the CO<sub>2</sub>-sensitive fluorophores (A<sub>4</sub>), while the luminescence of the reference luminophores  $(A_1, A_3)$  is not affected by changes in  $CO_2$ . In this case, the luminescence will be  $A_{on}$ = $A_1 + A_4$  and  $A_{off}$ =A<sub>3</sub>, when the LED is ON and OFF.

It is evident that luminescence parameters  $(A_1, A_2, A_3, A_4)$  are affected by the confounding factors individually. However, the ratio,  $A_{on}/A_{off}$ , yields a measure of  $CO_2$ , independent of the confounding factors since only the numerator changes with  $CO_2$ ; however, both sides of the fraction are equally affected by the confounding factors, resulting in a ratiometric measurement.

In f-DLR, the sensor is excited by a sinusoidal light wave. The luminescence components, in the f-DLR case, are visualized in Fig.1.b, as well as the overall signal. The overall signal can mathematically be expressed as,

$$A_{ovr}.cos\Phi_{ovr} = A_{lum}.cos\Phi_{lum} + A_{flu}.cos\Phi_{flu}, \quad (1)$$

$$A_{ovr}.sin\Phi_{ovr} = A_{lum}.sin\Phi_{lum} + A_{flu}.sin\Phi_{flu}, \quad (2)$$

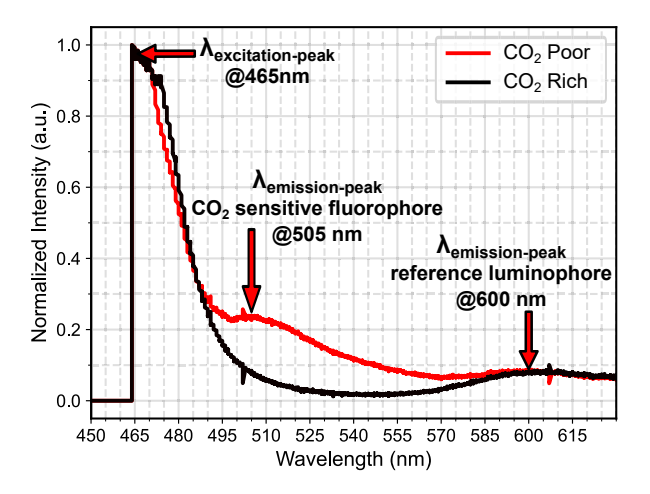


Fig. 2. Measured spectra of the luminescent sensing film emission under poor and a rich CO<sub>2</sub> environments.

where  $A_{ovr}$ ,  $A_{flu}$ ,  $A_{lum}$  and  $\Phi_{ovr}$ ,  $\Phi_{flu}$ ,  $\Phi_{lum}$  denote the amplitudes and phases of the overall signal, CO<sub>2</sub>-sensitive fluorophore, and reference luminophore, respectively. When the frequency of the excitation is slow, in the kHz range, there is no phase shift in the CO<sub>2</sub>-sensitive fluorophore,  $\Phi_{flu}$ =0, regardless of the PCO<sub>2</sub>. Therefore, terms  $\cos\Phi_{flu}$  in Eq. (1) and  $\sin\Phi_{flu}$  in Eq. (2) become 1 and 0, respectively.  $\Phi_{lum}$  is constant and not affected by the PCO<sub>2</sub> variations. Considering these facts, the ratio,  $\frac{Eq.~(1)}{Eq.~(2)}$ , results in

$$\frac{A_{ovr}.cos\Phi_{ovr}}{A_{ovr}.sin\Phi_{ovr}} = cot\Phi_{ovr} = cot\Phi_{lum} + \frac{1}{sin\Phi_{lum}} \cdot \frac{A_{flu}}{A_{lum}}.$$
 (3)

Hence, the phase shift of the overall signal,  $\Phi_{ovr}$ , depends only on the ratio of luminescent intensities of the CO<sub>2</sub>-sensitive fluorophore and reference luminophore.

In this paper, we explore both t-DLR and f-DLR techniques with an emphasis on the former. Our main goal is to implement a CO<sub>2</sub> monitoring prototype that can perform both DLR techniques in one design to quantify the relation of PCO<sub>2</sub> with the CO<sub>2</sub>-sensitive luminescence. We have used square pulses for the excitation to simplify the design and combine both techniques.

## III. SYSTEM ARCHITECTURE

#### A. Sensing Film

We have employed a CO<sub>2</sub>-sensitive luminescent film (SP-CD1T-D10-YAU-09NaCl, PreSens Precision Sensing) to perform DLR measurements. The sensing film is 10 mm in diameter and sensitive to up to 180 mmHg CO<sub>2</sub> [20]. Fig.2 illustrates the spectra of the sensing film measured with a Thorlabs CCS100 spectrometer in CO<sub>2</sub>-rich and -poor environments. As can be seen, the sensing film emits in two wavelengths when excited with the blue light of 465 nm wavelength. The emission peak of the CO<sub>2</sub>-sensitive fluorophore is at 505 nm, and the emission intensity decreases with increasing CO<sub>2</sub>. On the other hand, the reference luminophore emits at 600 nm, and its emission intensity is independent of CO<sub>2</sub> amount, obvious from Fig.2 and as described in Section II.

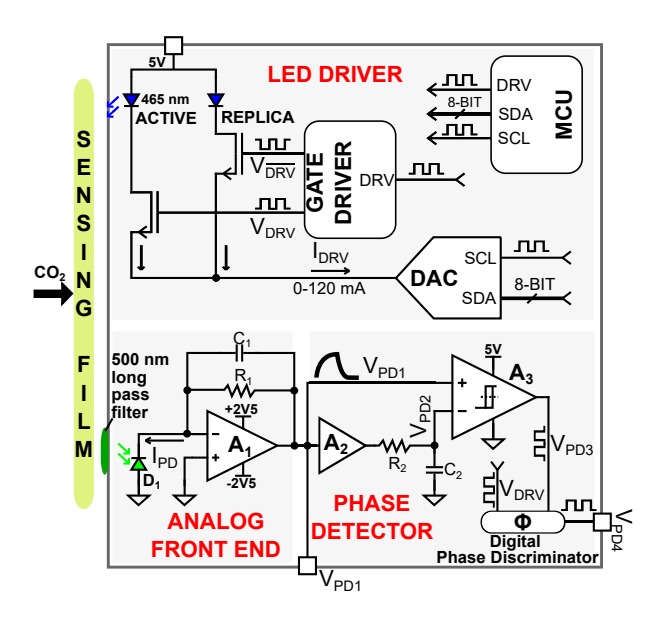


Fig. 3. Simplified schematic of the CO2 monitoring prototype.

#### B. Measurement Electronics

We have designed a  $CO_2$  monitoring prototype to evaluate the t-DLR and f-DLR techniques. The prototype, illustrated in Fig.3, is divided into three blocks: the LED driver, analog front end, and phase detector. The prototype is implemented in a 7 cm  $\times$  10 cm prototype circuit board (PCB) with off-theshelf components. As this PCB is designed as an evaluation board, multiple provisional components were not utilized in the measurements; however, they occupy space on the board. Without these provisions, the essential circuitry can fit into a smartwatch-sized board (approximately 3 cm  $\times$  4 cm).

The LED driver design is based on a current-sinking digital to analog converter (DAC). The current-sinking DAC sets the tail current ( $I_{DRV}$ ) of the MOSFET drivers, programmable via a 2-wire serial interface: serial data (SDA) and serial clock (SCL). An 8-bit SDA sets the tail current from 0 to 120 mA. The adjustability of the tail current provides complete control of the LED brightness and the ability to test the DLR techniques under varying excitation intensities. There are two MOSFET driver channels, the active and replica channel. The active channel drives the LED, which excites the sensing film, while the replica channel maintains the tail current flow when the active channel is off. The output current of the DAC settles in 250  $\mu$ s, so at least one channel should be on throughout the operation to overcome the settling time requirement of the DAC and to be able to create excitation pulses around tens of  $\mu$ s. We employed a gate driver with an inverting  $(V_{DRV})$  and a noninverting  $(V_{DRV})$  driver to switch between the active and replica channel. A microcontroller (MCU) generates the drive signal (DRV) with adjustable frequency and duty cycle. The MCU also generates the SDA and SCL to control the current sinking DAC. For the t-DLR technique, the drive signal is a pulse, while for the f-DLR, it is a continuous square wave.

The analog front end (AFE) converts the luminescence of the sensing film to a voltage through a photodiode (D<sub>1</sub>)

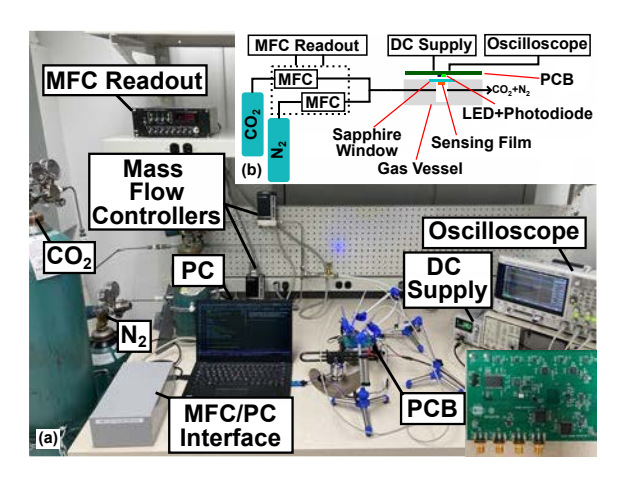


Fig. 4. (a) Image and (b) diagram of the test bench for the evaluation of the CO<sub>2</sub> monitoring prototype.

and a 500 nm long-pass filter, which blocks the excitation signal. The photodiode captures the luminescence and outputs a current  $(I_{PD})$  proportional to the luminescence intensity. A trans-impedance amplifier (TIA)  $(A_1)$  converts the photodiode current to a voltage  $(V_{PD1})$ . The  $R_1$  feedback resistor sets the trans-impedance gain, and the  $C_1$  compensation capacitor stabilizes the TIA. The output of the AFE,  $V_{PD1}$ , is captured by an oscilloscope and the data is saved into a universal serial bus (USB) device for performing the t-DLR technique.

The f-DLR technique quantifies the PCO<sub>2</sub> according to the phase shift in the luminescence signal. The f-DLR prototype employs a phase detector based on a digital phase discriminator with a 5 V transistor-transistor logic. The inputs of the phase discriminator are the active LED drive signal,  $V_{DRV}$ , and the logic-level shifted version of the AFE output,  $V_{PD3}$ .  $V_{DRV}$  serves as a reference signal to find the phase shift in the luminescence. The AFE output,  $V_{PD1}$ , a continuous square wave in the f-DLR technique, is buffered to a low-pass filter ( $R_2$ - $C_2$ ), which outputs the mean of  $V_{PD1}$ , only a DC component,  $V_{PD2}$ . Then,  $V_{PD1}$  and  $V_{PD2}$  are fed into a 5 V comparator, which gives  $V_{PD3}$ , the level-shifted version of  $V_{PD1}$ , with a 5 V logic required by the digital phase discriminator. The phase discriminator outputs a pulse train,  $V_{PD4}$ , the duty cycle of which is proportional to the phase difference between  $V_{DRV}$  and  $V_{PD3}$ .

#### IV. MEASUREMENT RESULTS

We observed the luminescence measured by the  $CO_2$  monitoring prototype under various  $CO_2$  levels using the test bench shown in Fig.4. The sensing film is placed in a gas vessel and excited through a sapphire window sealed to the vessel. The partial pressure of  $CO_2$  (PCO<sub>2</sub>) inside the vessel is adjusted by the mixture of two gases,  $CO_2$  and nitrogen (N<sub>2</sub>). The mass flow controllers (MFC) control the flow rate of each gas that sets the PCO<sub>2</sub> value.

#### A. t-DLR Measurement

In the t-DLR measurement, an LED pulse with 10  $\mu$ s width excites the sensing film. The AFE's output,  $V_{PD1}$ , is measured for 9 different PCO<sub>2</sub> values, ranging from 0 to 76 mmHg. The

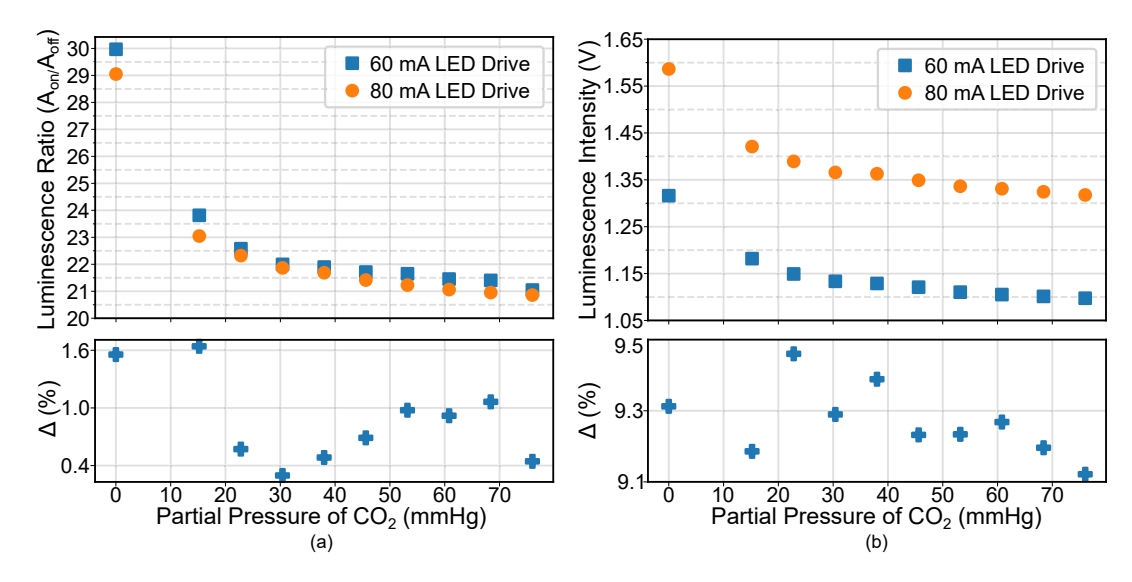


Fig. 5. (a) Luminescence ratio, and (b) intensity measured by the prototype for two distinct LED drive currents in 0-76 mmHg PCO<sub>2</sub> range.

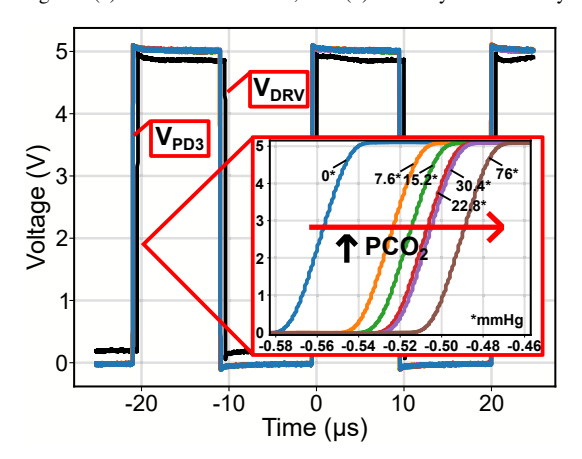


Fig. 6. LED drive signal,  $V_{DRV}$ , and the logic-level shifted luminescence,  $V_{PD3}$ , in 0-76 mmHg PCO<sub>2</sub> range.

ratio of the luminescence curve areas in each LED state and the luminescence ratio,  $(A_{on}/A_{off})$ , are calculated as described in Section II. We conducted this experiment with two distinct LED drive currents  $(I_{DRV})$ , 60 mA and 80 mA. Fig.5.a and Fig.5.b show the luminescence ratios and intensities for each case and the percentage variation  $(\Delta\%)$  between the LED drive currents, respectively. The t-DLR technique based on the luminescence ratio has a  $\Delta\%$  which is at most  $\sim 1.6\%$  across the PCO<sub>2</sub> range while the  $\Delta\%$  for the luminescence intensity is  $\sim 9.5\%$ , demonstrating the robustness of the t-DLR technique against the excitation strength variation.

### B. f-DLR Measurement

The excitation signal is a continuous square wave with a 50 kHz frequency in the case of the f-DLR measurement. Fig.6 demonstrates the inputs of the digital phase discriminator,  $V_{DRV}$  and  $V_{PD3}$ , under varying PCO<sub>2</sub> from 0 to 76 mmHg. Increasing carbon dioxide introduces a phase shift, consequently a time shift in  $V_{PD3}$ . However, the time shift is inconsistent across the PCO<sub>2</sub> values and in the ns range, defeating the purpose of the f-DLR technique. We suppose that

choosing a square wave instead of a sinusoidal wave as the excitation signal introduces an error in the phase measurement because of the harmonics present in the square wave [21], which we did not foresee. Nevertheless, the possibility of using a square wave excitation for the f-DLR technique and methods to compensate for the errors is a topic of future investigation.

TABLE I
COMPARISON OF PERFORMANCE PARAMETERS

Parameters	[22]	[12]	[23]	[24]	This Work
	2016	2020	2020	2021	2022
Modality Supply (V) Power (mW) Size (cm×cm) Bandwidth (Hz) Range (mmHg)	PetCO <sub>2</sub> NA 350 NA NA O-38	PtcCO <sub>2</sub> NA NA NA NA NA 30-50	PtcO <sub>2</sub> 1.8 0.631 IC 80 k 0-150	PtcO <sub>2</sub> 1.8-3 9 4×6 200 k 0-418	PtcCO <sub>2</sub> 5 541.25 7×10 1.15 M 0-75

NA: Not Addressed, IC: Integrated Circuit

Table I compares the the performance parameters of the designed prototype with the similar works in the literature. Since this application is a new research area, we have designed our prototype as an evaluation board to explore both DLR techniques, therefore the power and the size of our design are not optimized and can be reduced significantly by focusing on one DLR technique. Our design achieves the widest PCO<sub>2</sub> measurement range among the CO<sub>2</sub> monitors, 0-75 mmHg which covers the clinically significant range for healthy humans, 35-45 mmHg.

## V. CONCLUSION

We have explored both DLR techniques, namely t-DLR and f-DLR, to implement in a miniaturized  $PtCO_2$  monitoring prototype. The designed prototype successfully quantifies  $PCO_2$  in 0-76 mmHg range based on t-DLR technique. The measurement results have demonstrated that the prototype monitor is significantly less susceptible to the variations in the excitation intensity.

#### REFERENCES

- D. Castro and M. Keenaghan, "Arterial Blood Gas," in *StatPearls*. Treasure Island (FL): StatPearls Publishing, 2020. [Online]. Available: http://www.ncbi.nlm.nih.gov/books/NBK536919/
- [2] I. Costanzo, D. Sen, L. Rhein, and U. Guler, "Respiratory Monitoring: Current State of the Art and Future Roads," *IEEE Reviews in Biomedical Engineering*, vol. 15, pp. 103–121, 2022, conference Name: IEEE Reviews in Biomedical Engineering.
- [3] D. Sankaran, L. Zeinali, S. Iqbal, P. Chandrasekharan, and S. Lakshminrusimha, "Non-invasive carbon dioxide monitoring in neonates: methods, benefits, and pitfalls," *Journal of Perinatology*, pp. 1–10, Jun. 2021, bandiera\_abtest: a Cg\_type: Nature Research Journals Primary\_atype: Reviews Publisher: Nature Publishing Group Subject\_term: Laboratory techniques and procedures;Paediatrics;Respiratory tract diseases Subject\_term\_id: laboratory-techniques-and-procedures;paediatrics;respiratory-tract-diseases. [On-line]. Available: https://www.nature.com/articles/s41372-021-01134-2
- [4] U. Guler, D. Sen, I. M. Costanzo, T. B. Tufan, and L. Rhein, "Sensors for Neonatal Monitoring," in *Reference Module in Biomedical Sciences*. Elsevier, Jan. 2022. [Online]. Available: https://www.sciencedirect.com/ science/article/pii/B9780128225486001047
- [5] K. P. Sullivan, H. O. White, L. E. Grover, J. J. Negron, A. F. Lee, and L. M. Rhein, "Transcutaneous carbon dioxide pattern and trend over time in preterm infants," *Pediatric Research*, pp. 1–7, Jan. 2021, publisher: Nature Publishing Group. [Online]. Available: http://www.nature.com/articles/s41390-020-01308-2
- [6] U. Guler, I. Costanzo, and D. Sen, "Emerging Blood Gas Monitors: How They Can Help With COVID-19," *IEEE Solid-State Circuits Magazine*, vol. 12, no. 4, 2020.
- [7] M. Dicembrino, I. A. Barbieri, C. Pereyra, and V. Leske, "End-tidal CO2 and transcutaneous CO2: Are we ready to replace arterial CO2 in awake children?" *Pediatric Pulmonology*, vol. 56, no. 2, pp. 486–494, 2021, \_eprint: https://onlinelibrary.wiley.com/doi/pdf/10.1002/ppul.25217. [Online]. Available: http://onlinelibrary.wiley.com/doi/abs/10.1002/ppul.25217
- [8] M. Contini, A. Angelucci, A. Aliverti, P. Gugliandolo, B. Pezzuto, G. Berna, S. Romani, C. C. Tedesco, and P. Agostoni, "Comparison between PtCO2 and PaCO2 and Derived Parameters in Heart Failure Patients during Exercise: A Preliminary Study," Sensors, vol. 21, no. 19, p. 6666, Oct. 2021. [Online]. Available: https://www.mdpi.com/1424-8220/21/19/6666
- [9] J. W. Severinghaus, "A combined transcutaneous PO2-PCO2 electrode with electrochemical HCO3- stabilization," *Journal of Applied Physiology*, vol. 51, no. 4, pp. 1027–1032, Oct. 1981. [Online]. Available: https://www.physiology.org/doi/10.1152/jappl.1981.51.4.1027
- [10] T. B. Tufan, D. Sen, and U. Guler, "An Infra-Red-Based Prototype for a Miniaturized Transcutaneous Carbon Dioxide Monitor," in 2021 43rd Annual International Conference of the IEEE Engineering in Medicine Biology Society (EMBC), Nov. 2021, pp. 7132–7135, iSSN: 2694-0604.
- [11] V. V. Tipparaju, S. J. Mora, J. Yu, F. Tsow, and X. Xian, "Wearable Transcutaneous CO2 Monitor Based on Miniaturized Nondispersive Infrared Sensor," *IEEE Sensors Journal*, pp. 1–1, 2021, conference Name: IEEE Sensors Journal.
- [12] P. Grangeat, S. Gharbi, A. Koenig, M.-P. Comşa, M. Accensi, H. Grateau, A. Ghaith, S. Chacaroun, S. Doutreleau, and S. Vergès,

- "Evaluation in Healthy Subjects of a Transcutaneous Carbon Dioxide Monitoring Wristband during Hypo and Hypercapnia Conditions\*," in 2020 42nd Annual International Conference of the IEEE Engineering in Medicine Biology Society (EMBC), Jul. 2020, pp. 4640–4643, iSSN: 2694-0604.
- [13] T. B. Tufan and U. Guler, "A Fluorescent Thin Film-Based Miniaturized Transcutaneous Carbon Dioxide Monitor," in 2021 IEEE Biomedical Circuits and Systems Conference (BioCAS), Oct. 2021, pp. 1–5, iSSN: 2163-4025.
- [14] J. P. Cascales, X. Li, E. Roussakis, and C. L. Evans, "A Patient-Ready Wearable Transcutaneous CO2 Sensor," *Biosensors*, vol. 12, no. 5, p. 333, May 2022, number: 5 Publisher: Multidisciplinary Digital Publishing Institute. [Online]. Available: https://www.mdpi.com/2079-6374/12/5/333
- [15] M. Xu, B. Peng, X. Zhu, and Y. Guo, "Multi-Gas Detection System Based on Non-Dispersive Infrared (NDIR) Spectral Technology," Sensors, vol. 22, no. 3, p. 836, Jan. 2022. [Online]. Available: https://www.mdpi.com/1424-8220/22/3/836
- [16] L. Zhou, Y. He, Q. Zhang, and L. Zhang, "Carbon Dioxide Sensor Module Based on NDIR Technology," *Micromachines*, vol. 12, no. 7, p. 845, Jul. 2021, number: 7 Publisher: Multidisciplinary Digital Publishing Institute. [Online]. Available: https://www.mdpi.com/2072-666X/12/7/845
- [17] J. R. Lakowicz, Principles of fluorescence spectroscopy, 3rd ed. New York: Springer, 2006.
- [18] M. Čajlaković, A. Bizzarri, and V. Ribitsch, "Luminescence lifetime-based carbon dioxide optical sensor for clinical applications," *Analytica Chimica Acta*, vol. 573-574, pp. 57–64, Jul. 2006. [Online]. Available: https://www.sciencedirect.com/science/article/pii/S0003267006011536
- [19] I. Klimant, C. Huber, G. Liebsch, G. Neurauter, A. Stangelmayer, and O. S. Wolfbeis, "Dual Lifetime Referencing (DLR) a New Scheme for Converting Fluorescence Intensity into a Frequency-Domain or Time-Domain Information," in New Trends in Fluorescence Spectroscopy: Applications to Chemical and Life Sciences, ser. Springer Series on Fluorescence, B. Valeur and J.-C. Brochon, Eds. Berlin, Heidelberg: Springer, 2001, pp. 257–274. [Online]. Available: https://doi.org/10.1007/978-3-642-56853-4\_13
- [20] CO2 Sensor Spots CD1, Presens Precision Sensing, 2016.
- [21] S. Subhan and S. Ha, "Harmonic Error Cancellation for Accurate Square-wave-based Bio-Impedance Measurements," in 2018 40th Annual International Conference of the IEEE Engineering in Medicine and Biology Society (EMBC), Jul. 2018, pp. 4273–4276, iSSN: 1558-4615.
- [22] T. Vincent and J. Gardner, "A low cost MEMS based NDIR system for the monitoring of carbon dioxide in breath analysis at ppm levels," *Sensors and Actuators B: Chemical*, vol. 236, pp. 954–964, Nov. 2016. [Online]. Available: https://linkinghub.elsevier.com/retrieve/pii/ S0925400516304798
- [23] I. Costanzo, D. Sen, and U. Guler, "An Integrated Readout Circuit for a Transcutaneous Oxygen Sensing Wearable Device," in 2020 IEEE Custom Integrated Circuits Conference (CICC). IEEE, Mar. 2020, pp. 1–4. [Online]. Available: https://ieeexplore.ieee.org/document/9075881/
- [24] I. Costanzo, D. Sen, J. Adegite, P. M. Rao, and U. Guler, "A Noninvasive Miniaturized Transcutaneous Oxygen Monitor," *IEEE Transactions on Biomedical Circuits and Systems*, 2021.